Luminescent Silver Sulfide Clusters

Dominik Brühwiler, Claudia Leiggener, Stephan Glaus, and Gion Calzaferri*

Department of Chemistry and Biochemistry, University of Bern, Freiestrasse 3, CH-3000 Bern 9, Switzerland

Received: June 26, 2001; In Final Form: October 5, 2001

Silver sulfide clusters are synthesized in the cavities of sodium and calcium zeolite A microcrystals by exposing the activated Ag^+-loaded zeolite to H_2S. The growth of the silver sulfide clusters during rehydration of the samples is investigated by means of diffuse reflectance spectroscopy. Monomers of Ag_2S are formed at low Ag^+-loading through reaction of AgSH molecules, yielding colorless composites, which exhibit a characteristic blue-green photoluminescence. Yellow colored samples showing an orange-red luminescence with an average decay time of 81 μs (−160 °C) are obtained at medium silver sulfide content. Further increasing the silver sulfide loading and therefore the cluster size causes a bathochromic shift of this emission which is accompanied by a shortening of the luminescence lifetime. The samples generally exhibit large Stokes-shifts, which can be attributed to HOMO−LUMO transitions with small oscillator strengths. The Ag_2S−zeolite host−guest system constitutes a three-dimensional array of silver sulfide clusters. The experimental data and results from quantum chemical calculations suggest that the optical absorption and luminescence properties of this material are mainly due to the presence of isolated silver sulfide clusters inside the zeolite cavities. The characteristics of the composites are thereby to a certain extent influenced by the cocations. Most remarkably, stronger luminescence, visible at room temperature, could be observed for silver sulfide clusters in calcium zeolite A compared to clusters in sodium zeolite A.

Introduction

The synthesis and the properties of semiconductor particles in the size regime of a few to hundreds of angstroms continues to attract considerable interest.[1] Significant quantum confinement effects can be observed in clusters made from II−VI or IV−VI compounds such as CdS[2], CdSe[3], ZnO,[4] ZnS,[5] or PbS.[6] While excellent progress has been made in the preparation and characterization of these materials, very little is known about the properties of small Ag_2S species. This can be partly attributed to the fact that silver sulfide clusters show a strong tendency to aggregate into bulk, which complicates their synthesis considerably.

The low-temperature phase of bulk silver sulfide is stable up to approximately 177 °C and is usually denoted as α-Ag_2S. Historically, we can go as far back as 1833 when Michael Faraday made the remarkable discovery that silver sulfide behaves as an insulator at room temperature but exhibits high electrical conductivity at elevated temperatures, leading him to the following conclusion: *"There is no other body with which I am acquainted, that, like sulfuret of silver, can compare with metals in conducting power for electricity of low tension when hot, but which, unlike them, during cooling, loses in power, while they, on the contrary, gain. Probably, however, many others may, when sought for, be found".*[7] Today it is well-known that α-Ag_2S is a semiconductor with a monoclinic structure[8] and a band gap of approximately 1 eV at room temperature.[9] The electronic transition from the valence band to the conduction band is essentially a charge transfer from 3p(S) to 5s(Ag) orbitals.[10] Bulk silver sulfide has been considered for photoimaging and photodetection in the IR,[11] while small clusters are known to play an important role in photographic sensitivity.[12−15]

It has been reported that silver sulfide clusters with sizes ranging from 23 to 76 Å can be synthesized in reverse micelles.[16] Another method utilizes the rapid expansion of a $AgNO_3$ solution in supercritical ammonia into an ethanol solution of Na_2S. An average diameter of 73 Å was found after stabilizing the thus formed particles with a suitable polymer.[17] Dosed addition of a $AgNO_3$ solution to a gelatin solution containing Na_2S was reported to yield silver sulfide clusters in the size regime between 30 and 100 Å.[18] Other methods use nylon thin films (cluster size ranging from 47 to 112 Å),[19] Nafion membranes (cluster size ranging from 50 to 150 Å)[20] or capping with cysteine/glutathione (average cluster size of 90 Å)[21] to stabilize the silver sulfide clusters. Some of the results obtained by the above-mentioned methods suggest the presence of a quantum size effect for silver sulfide clusters with a diameter between 20 and 100 Å (see refs 17, 18, 21, and 22), while other reports clearly negate the presence of such an effect (see, e.g., ref 19). There is to our knowledge no reliable information about the effective masses of the electrons and holes in silver sulfide. It is therefore to date not possible to estimate the optimum cluster size for excitonic confinement.

We recently reported the synthesis of silver sulfide particles in the cavities of sodium zeolite A.[10] By using this preparation method it is possible to produce particles in the size regime below 15 Å. The synthesis can be divided into four steps: (i) loading of the zeolite with Ag^+, (ii) activation of the Ag^+-loaded zeolite, (iii) reaction with H_2S, and (iv) rehydration. We now present experimental results that lead to the derivation of a mechanism for the cluster growth inside the zeolite cavities and investigate the pronounced photoluminescence properties of the thus formed silver sulfide species. The steady-state and time-resolved luminescence behavior of differently loaded zeolite samples is discussed and the influence of the co-cations on the properties of the composites is illustrated by comparison of the

* Corresponding author. E-mail: gion.calzaferri@iac.unibe.ch.

10.1021/jp012453b CCC: $22.00
Published on Web 03/21/2002

luminescence spectra of clusters in sodium and calcium zeolite A. The use of zeolite A as a host yields three-dimensional arrays of silver sulfide clusters. The role of long-range interactions in such a system is discussed by means of MO calculations, which are furthermore applied to study the nature of the electronic transitions in small silver sulfide species.

Experimental Section

Nomenclature. The following abbreviations are used: NaA for sodium zeolite A ($Na_{12}[(AlO_2)_{12}(SiO_2)_{12}]$) and CaA for calcium zeolite A ($Ca_6[(AlO_2)_{12}(SiO_2)_{12}]$). The stoichiometry of the silver sulfide zeolite A composites is $Ag_xS_{x/2}Na_{12-x}H_xSi_{12}Al_{12}O_{48}\cdot nH_2O$ for clusters in NaA and $Ag_xS_{x/2}Ca_{6-x/2}H_xSi_{12}Al_{12}O_{48}\cdot nH_2O$ for clusters in CaA (pseudo unit cell contents). We use the abbreviations Ag_2S-NaA-*x* and Ag_2S-CaA-*x* for the differently loaded samples, where *x* denotes the number of silver ions per α-cage of zeolite A.

Synthesis of NaA and CaA. Commercial zeolite A usually contains traces of iron and chloride and is therefore not suitable for applications which rely on the characterization by sensitive spectroscopic methods. Chemically pure and highly crystalline NaA was synthesized and characterized according to ref 23. Crystals with an average dimension of 3 μm are obtained by this method. CaA was prepared by suspending 500 mg of NaA in 20 mL of a 0.5 M $Ca(NO_3)_2$ solution (Merck, p.a.) for 15 min at room temperature (repeat two times). Thereafter, the samples were washed three times with 20 mL of bidistilled water.

Preparation of Ag^+-Loaded NaA. A 120 mg amount of NaA was finely dispersed in 10 mL of bidistilled water. A calculated volume of a 0.1 M $AgNO_3$ solution (Merck, Titrisol) was added to obtain the desired silver loading. Quantitative uptake of Ag^+ can be assumed for loading levels up to 6 Ag^+ per α-cage.[24,25] After shaking the suspension for 30 min at room temperature, the zeolite was centrifuged off and washed two times with 15 mL of bidistilled water.

Preparation of Ag^+-Loaded CaA. In this case, a quantitative uptake of Ag^+ can only be assumed for loading levels up to approximately one Ag^+ per α-cage. For higher loading levels the required volume of 0.1 M $AgNO_3$ solution was deduced from a previously measured exchange isotherm.[26] Furthermore, equilibration times of a few hours had to be taken into account.

Activation of the Ag^+-Loaded Zeolites. The samples were activated at room temperature under high vacuum for 40−60 h (final pressure $(4-7)\times10^{-7}$ mbar). The color changes observed during this process, which simply corresponds to the dehydration of the silver ions inside the zeolite cages, and the electronic absorption spectra of activated Ag^+-loaded zeolite A have been reinvestigated recently.[26,27]

Reaction with H_2S and Rehydration. The activated samples were exposed to approximately 80 mbar of H_2S (Messer Griesheim) for 1 h, subsequently evacuated overnight to remove excess H_2S and finally rehydrated under ambient conditions.

Physical Measurements. The integrity of the samples was verified by scanning electron microscopy (SEM) and X-ray powder diffraction (XRD). Diffuse reflectance spectra were recorded at room temperature using a Perkin-Elmer Lambda 14 spectrophotometer equipped with an integrating sphere (Labsphere RSA-PE-20). The data were converted using the Kubelka−Munk formula. Since the scattering coefficient of zeolite is gradual in the wavelength region of interest, the Kubelka−Munk function is a good representation of the absorption spectrum. For the measurement of photoluminescence, layers (between 100 and 200 μm thick) of the fully hydrated samples were prepared on quartz plates. The zeolite material under investigation was therefore dispersed in bidistilled water by sonification and dripped on the freshly cleaned support. Evaporation of the solvent under ambient conditions lead to the formation of an adhesive polygrain layer. Photoluminescence measurements were carried out on fully hydrated samples only. Steady-state luminescence spectra were taken on a Perkin-Elmer LS 50B spectrofluorometer equipped with a nitrogen cryostat (Oxford Instruments PE 1704). Time-resolved luminescence measurements were performed by exciting the samples with a pulsed laser (5 ns, 4−5 mJ/pulse) at 440 nm. The system used for this purpose consists of a Nd:YAG laser (Quantel Brilliant) and an OPO (Opotek MagicPrism Vibrant Vis) which is pumped by the third harmonic of the Nd:YAG. A sample compartment similar to the one described in an earlier report[28] was utilized. The setup includes a gated OMA III system for detection (EG&G PARC, 1455R-700-HQ detector). Alternating spectrum scans and background scans were collected and the background corrected spectra were added (typically 100). Spectrum scans were triggered by the excitation pulse, while a signal provided by a digital delay (Stanford Research Systems Inc. DG535) was used to initiate the background scans. Spectra were taken at 51 different points of time after excitation with a constant increment of approximately one tenth of the corresponding average luminescence lifetime. To determine the luminescence decay curves of the Ag_2S-CaA-*x* samples ($x \geq 2$), the time-dependent spectra were integrated from 500 to 820 nm.

MO and Oscillator Strength Calculations. Extended Hückel molecular orbital (EHMO) calculations[29] in their ASED (atomic superposition and electron delocalization) form[30] were carried out with the ICON-EDiT program package.[31] The off-diagonal elements were calculated as follows:

$$H_{ij} = \frac{1}{2}KS_{ij}(H_{ii} + H_{jj}) \tag{1}$$

To determine the Wolfsberg−Helmholz parameter *K*, the weighted formula[32] was used in a distance-dependent form:[33]

$$K = 1 + k\left(\frac{\exp(-\delta(R - d_0))}{1 + (\delta(R - d_0 - |R - d_0|))^2}\right) \tag{2}$$

with

$$k = \kappa + \Delta^2 - \Delta^4\kappa \qquad \text{and} \qquad \Delta = \frac{H_{ii} - H_{jj}}{H_{ii} + H_{jj}} \tag{3}$$

whereas $\kappa = 0.8$ and $\delta = 0.35$ Å^{-1}.[34] Equations 1−3 are the defaults implemented in ICON-EDiT. H_{ii} and H_{jj} are the Coulomb integrals of the *i*th and *j*th atomic orbital and have been determined by charge iteration; for details see refs 31, 34, and 35. *R* is the distance between the atoms on which the atomic orbitals are located. d_0 is the sum of the *i*th and *j*th atomic orbital radii calculated from the corresponding Slater exponents using eqs 13 and 14 in ref 30. The Slater parameters used for calculation are listed in Table 1.

Calculations of the oscillator strength of electronic dipole-induced transitions based on EHMO wave functions were performed using the program EDiT which is part of the ICON-EDiT package.[31,36]

Band Structure Calculations. Extended Hückel tight-binding[37] band structure calculations in their ASED form were carried out using BICON−CEDiT.[38] The off-diagonal elements

TABLE 1: Slater Exponents Used for EHMO Calculations

element	AO	ζ_1	ζ_2	c_1	c_2
Ag	5s	1.85			
	5p	1.30			
	4d	3.91	1.54	0.824	0.329
S	3s	2.28			
	3p	1.82			
Na	3s	0.82			
	3p	0.82			
H	1s	1.30			

were calculated according to eqs 1−3 with the same parameters as in the MO calculations.

Results and Discussion

Mechanism of Cluster Growth. We start by examining the formation of silver sulfide clusters in zeolite samples with a low content of Ag^+, e.g., 0.05 Ag^+ per α-cage. The silver ions are evenly distributed among the α-cages, implying that only 5% actually contain a silver ion in this case (see Figure 3 in ref 27). Activation of the Ag^+-loaded zeolite and subsequent adsorption of H_2S leads to the following reaction inside an α-cage:

$$Ag^+ + H_2S \rightleftharpoons AgSH + H^+ \quad (4)$$

It can be assumed that the silver atom of the thus formed AgSH molecule is at this stage still coordinated to zeolite framework oxygen atoms. Uptake of water during rehydration mobilizes the AgSH molecules through solvatation. Encounter of two AgSH molecules causes the following reaction:

$$AgSH + AgSH \rightleftharpoons Ag_2S + H_2S \quad (5)$$

H_2S escapes from the zeolite. Further diffusion of the Ag_2S molecules might be possible, but is expected to occur at a much slower rate due to stronger sterical hindrance.

We now present the experimental evidence on which the above stated mechanism is based. Figure 1 shows the diffuse reflectance spectra of two freshly prepared samples of Ag_2S−NaA-0.05 at different times during rehydration. It has to be noted that pure NaA (and also CaA) shows no absorption in the investigated spectral range (see Figure 2 in ref 27), whereas the spectra of fully hydrated Ag^+-loaded zeolite samples contain a band around 225 nm, which is attributed to a charge-transfer transition from Ag^+-coordinated water molecules to the empty 5s orbital of Ag^+.[26,34] Due to the low loading level, no absorption could be detected in the hydrated and also in the activated state of NaA containing 0.05 Ag^+ per α-cage. The observed bands shown in Figure 1 can therefore be ascribed to the presence of sulfide or hydrosulfide species.

The adsorption of H_2S on activated Ag^+-loaded NaA does not only cause the formation of silver sulfide and silver hydrosulfide species but in addition leads to the dissociation of H_2S on those sodium ions which act as strong sorption centers (Na^+ located at 4-ring and 8-ring sites). The thus formed Na^+-SH^- and Na^+-S^{2-} pairs can be identified by a charge-transfer transition in the UV region. Such an effect has already been observed in sodium zeolite X.[39] Similar absorption bands can also be found in spectra of concentrated solutions of NaOH containing sulfides.[40] Figure 2 shows the diffuse reflectance spectra of NaA after adsorption of H_2S at different times during rehydration. It confirms the assignment of the band at 225 nm to Na^+-SH^- and Na^+-S^{2-} species. Rehydration causes protonation of these species and subsequent release of H_2S. The

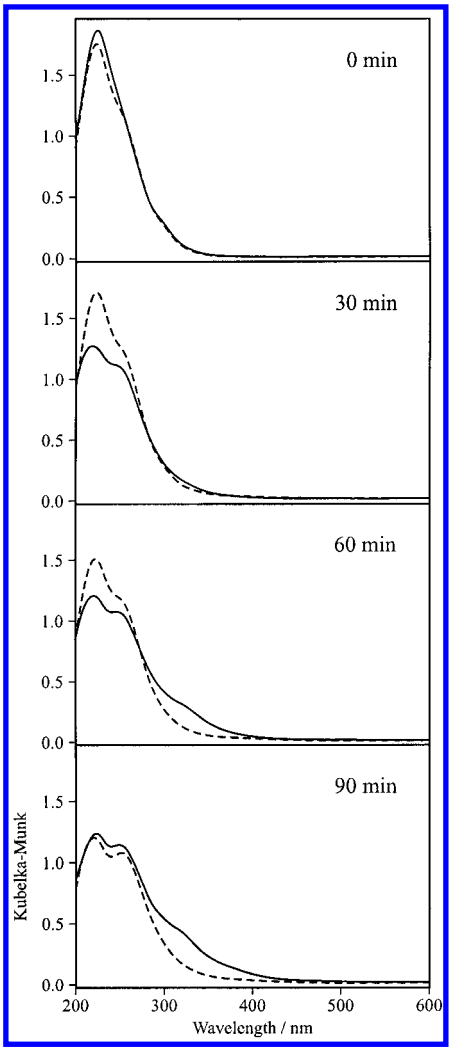

Figure 1. Diffuse reflectance spectra of Ag_2S−NaA-0.05 at different times during rehydration over silica gel (dashed lines) and under 92% humidity (solid lines).

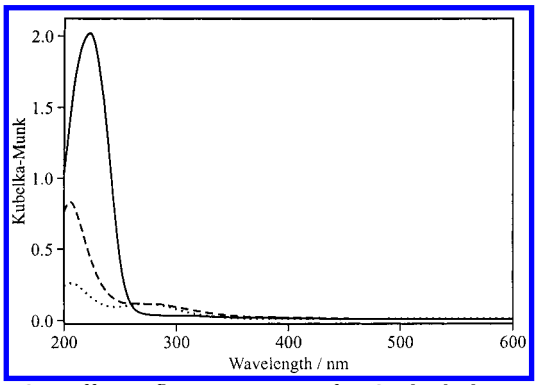

Figure 2. Diffuse reflectance spectra of H_2S adsorbed on NaA at different times during rehydration: 0 min (solid), 60 min (dashed), and 210 min (dotted).

residual absorption bands after complete rehydration can be attributed to strongly bound sulfide species. At this point it should be noted, that dissociative adsorption of H_2S does not take place in pure CaA. This is due to the lack of strong sorption centers in this zeolite (all Ca^{2+} occupy 6-ring sites). The evolution of H_2S by Ag_2S−CaA samples during rehydration is therefore solely caused by reactions of the type described by eq 5.

Formation of silver sulfide clusters (including monomers of Ag_2S) is indicated by the evolution of a band at wavelengths

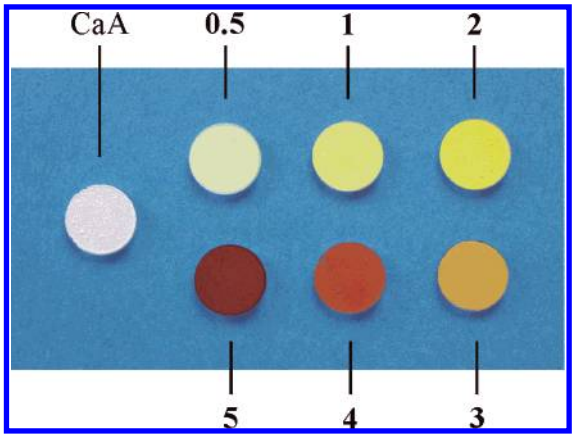

Figure 3. Photographic picture of fully hydrated Ag_2S-CaA samples. The samples are labeled with the corresponding average number of Ag^+ per α-cage. The sample on the left is pure calcium zeolite A.

longer than approximately 300 nm. With increasing silver sulfide content this absorption band increasingly dominates the diffuse reflectance spectrum.[10] As can be seen in Figure 1, the rate at which this band develops depends on the availability of water. Once formed inside the zeolite cavities, the silver sulfide clusters are stable even after repeated evacuation and rehydration steps, whereas activation and reaction with H_2S reverses the cluster formation. The band around 320 nm first disappears and then reappears during rehydration. Note that this is just the back reaction of eq 5, which applies for larger clusters as well. Samples with one or more Ag^+ per α-cage already feature a long wavelength band before rehydration. This can be attributed to the high local concentration of silver ions which allows the formation of clusters immediately after reaction with H_2S.[10]

The appearance of the Ag_2S-NaA and Ag_2S-CaA samples depends on the silver sulfide content. The color varies from colorless (low content) to yellow (medium content) to brown (high content). Figure 3 shows Ag_2S-CaA samples after completion of the rehydration process. Keep in mind that Ag^+-loaded zeolite A is colorless in the fully hydrated state.[26,27] The color of the samples shown in Figure 3 is solely caused by the presence of silver sulfide clusters in the zeolite cavities.

The zeolite framework prevents the silver sulfide clusters from aggregating. This stabilizing effect can be illustrated by dissolving Ag_2S-NaA or Ag_2S-CaA in 0.1 M hydrochloric acid. Formation of a black precipitate is observed upon decomposition of the zeolite. This precipitate is identified by XRD as α-Ag_2S. A problem encountered in the preparation of Ag_2S-NaA samples (especially at high loading levels) is the formation of α-Ag_2S on the outer surface of the zeolite crystals upon exposing the activated Ag^+-loaded zeolite to H_2S. This undesirable effect can be significantly diminished by using CaA instead of NaA. The number of free coordination sites for exchangeable cations is much larger in CaA than in NaA. It can therefore be expected that the mobility of silver ions in CaA is strongly reduced compared to NaA, thus preventing the inserted Ag^+ from diffusing to the outer surface of the zeolite crystals during activation. The improved quality of the Ag_2S-CaA samples is particularly evident at loading levels of more than one Ag^+ per α-cage.

Photoluminescence. In a previous communication, we reported the luminescence spectra of Ag_2S-NaA samples.[10] Ag_2S-CaA samples exhibit comparatively much stronger luminescence, visible at room temperature. Figure 4 shows the luminescence spectra of Ag_2S-CaA samples with varying silver sulfide content.

Comparison of the spectra shown in Figure 4 with the previously reported spectra of Ag_2S-NaA samples reveals the following similarities: A low silver sulfide content is characterized by a blue-green emission (480 nm for Ag_2S-NaA and 490 nm for Ag_2S-CaA) and a corresponding excitation spectrum with distinct and narrow bands (see Figure 5). The Stokes shift is 1.3 eV. Interpretation of these bands is not straightforward, since no reports on the properties of small silver sulfide clusters are available up to now. Given the distinct nature of the excitation bands and the low silver sulfide content, it can be concluded that the blue-green luminescence is caused by species with molecular properties, most likely monomers of Ag_2S. At higher loading levels, an orange-red luminescence becomes increasingly dominant. The excitation spectrum for this emission is broad and unstructured (see Figure 5) and can therefore be attributed to larger clusters. Given the dimensions of an α-cage, it can be assumed that the largest silver sulfide cluster that fits into this cavity would have a stoichiometry close to Ag_8S_4. The structure of such a cluster and also of smaller silver sulfide species is difficult to predict. Quantum chemical calculations suggest that a variety of energetically favorable geometries are possible already for Ag_4S_2.[41]

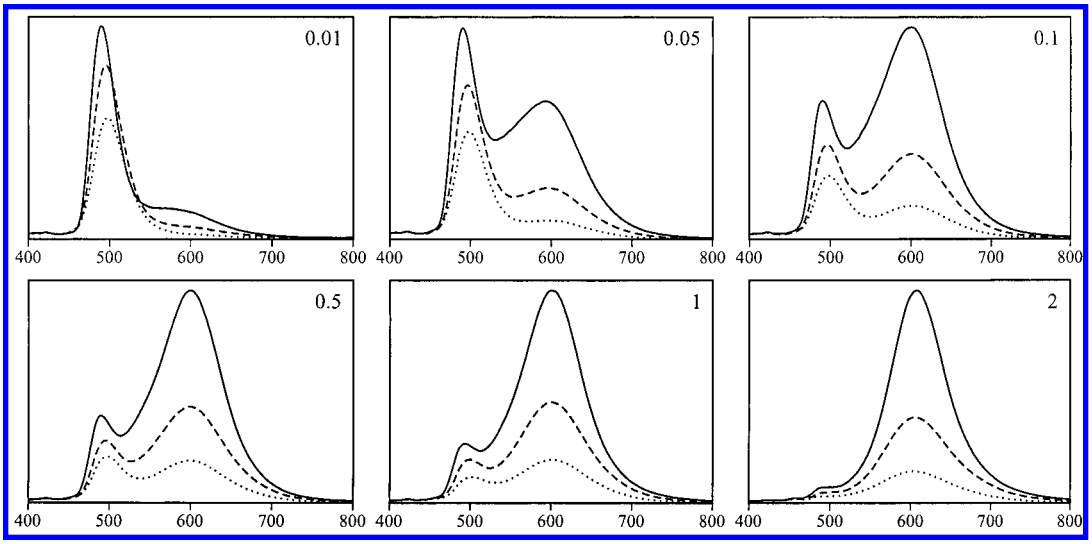

Figure 4. Luminescence spectra of Ag_2S-CaA samples at −195 °C (solid lines), −100 °C (dashed lines) and −50 °C (dotted lines). The abscissa and the ordinate give the wavelength in nanometers and the emission intensity, respectively. The spectra are labeled with the corresponding average number of Ag^+ per α-cage. Excitation was performed at 280 nm.

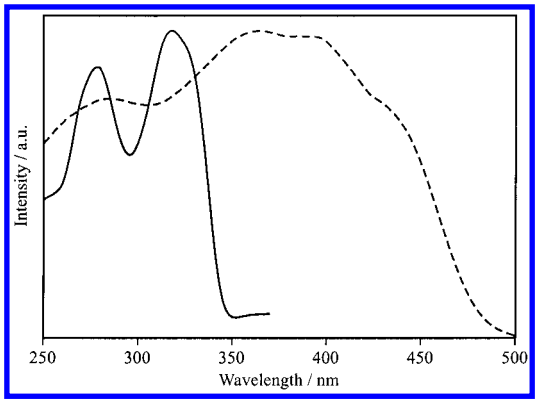

Figure 5. Excitation spectra of Ag_2S-CaA-0.05 (solid) and Ag_2S-CaA-2 (dashed) at −195 °C. Emission was observed at the maximum of the corresponding luminescence band. The spectra are scaled to equal heights.

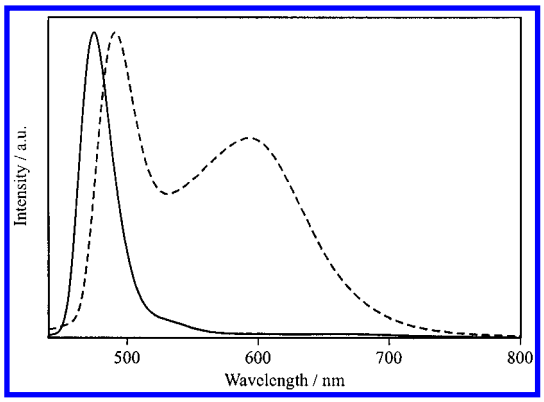

Figure 6. Luminescence spectra of Ag_2S-NaA-0.05 (solid) and Ag_2S-CaA-0.05 (dashed) at −195 °C. Excitation was performed at 280 nm.

The cocations do not only influence the outer surface quality of the samples but also the cluster growth inside the cavities. Figure 6 compares the luminescence spectra of Ag_2S-NaA-0.05 and Ag_2S-CaA-0.05. It seems that the formation of larger clusters is less favorable in NaA. This can be attributed to the smaller pore size of this zeolite, given by the fact that the windows between the α-cages are partially blocked by sodium cations. This inhibits the diffusion of small silver sulfide and silver hydrosulfide species and therefore limits the cluster growth.

The luminescence spectra of Ag_2S-NaA samples with medium silver sulfide content contain essentially three bands: The already mentioned blue-green and orange-red bands and furthermore a yellow emission at 530 nm (see Figure 4 in ref 10). The latter cannot be immediately observed in Ag_2S-CaA samples (see Figure 4). Decomposition of the luminescence spectrum of Ag_2S-CaA-0.05 into three Gaussian curves reveals that such a band might nonetheless exist (see Figure 7), being obscured by the red-shifted blue-green and by the blue-shifted orange-red emission bands (with respect to the corresponding bands in Ag_2S-NaA). Considering the dependence of the intensity of the yellow emission band upon the silver sulfide content, it can be concluded that this luminescence is caused by a cluster of intermediate size.

We have so far discussed the luminescence properties of Ag_2S-NaA and Ag_2S-CaA samples with loading levels of up to two Ag^+ per α-cage. By using CaA as host material it is possible to produce luminescent samples with even higher silver sulfide content. Figure 8 shows the low-temperature luminescence spectra of Ag_2S-CaA-2, Ag_2S-CaA-4, and Ag_2S-CaA-6. These samples only exhibit the long wavelength emission,

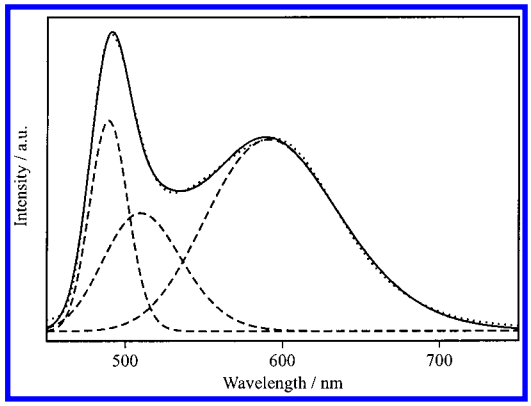

Figure 7. Luminescence spectrum of Ag_2S-CaA-0.05 (dotted) and its decomposition into three Gaussian curves (dashed). The solid line corresponds to the sum of the Gaussian curves.

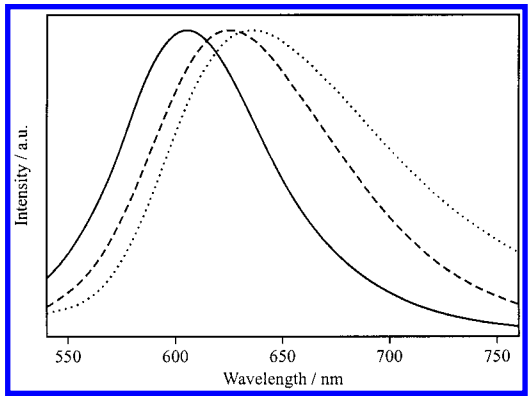

Figure 8. Luminescence spectra of Ag_2S-CaA-2 (solid), Ag_2S-CaA-4 (dashed), and Ag_2S-CaA-6 (dotted) at −195 °C. Excitation was performed at 280 nm. The spectra are scaled to identical heights.

which is red-shifted with increasing silver sulfide content. This effect is accompanied by a shortening of the luminescence lifetime. The following average decay times were measured for Ag_2S-CaA-x samples at −160 °C: 81 μs ($x = 2$), 49 μs ($x = 3$), 26 μs ($x = 4$), 9 μs ($x = 5$), and 2 μs ($x = 6$). The mechanism that causes this increased quenching at high loading levels is not yet completely understood. We have pointed out that a higher silver sulfide content leads to the formation of larger clusters. It can further be assumed that short-range interactions between clusters in adjacent α-cages are possible at high loading levels. Such interactions could generate new pathways for the radiationless deactivation of the excited cluster states.

The luminescence decays are multiexponential due to the heterogeneous nature of the Ag_2S-CaA samples. Two main components can be identified in the luminescence decay of Ag_2S-CaA-2 at −160 °C. As can be seen in Figure 9, the high energy part of the luminescence spectrum of Ag_2S-CaA-2 is dominated by the slower component (75 μs) and the low energy part by the faster component (10 μs). Analysis of the luminescence decay by the exponential series method revealed that these components are the centers of two broad lifetime distributins.

Three reasons can cause the observed heterogeneity: (i) several accessible electronic states within a narrow energy range, (ii) distribution of luminescent species among different coordination sites, (iii) different luminescent species. The comparatively narrow emission band, which is exhibited by Ag_2S-CaA-2, suggests a small number of different species in this case.

Theoretical Considerations

Our interpretation of the diffuse reflectance spectra in Figure 1 is supported by the results of MO calculations. We first

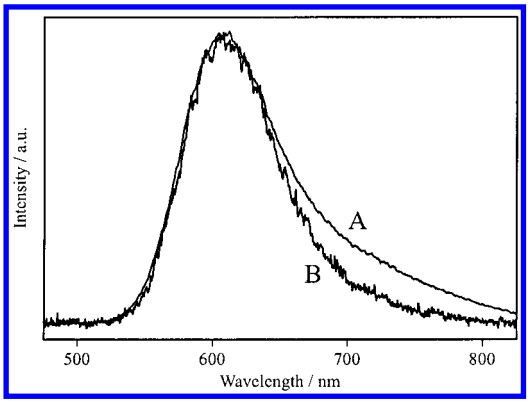

Figure 9. Luminescence spectra of Ag_2S−CaA-2 at different times after pulsed excitation at 440 nm: 0−8 μs (spectrum A) and 200−208 μs (spectrum B). The spectra were measured at −160 °C and are scaled to identical heights.

TABLE 2: Bond Lengths and Angles

molecule	bond angle/deg	bond	length/Å
Ag_2S	112	Ag−S	2.42
AgSH	105	Ag−S	2.32
		S−H	1.33
NaSH	180	Na−S	2.32
		S−H	1.34

TABLE 3: Calculated Major Electronic Transitions in Monomers of Ag_2S, AgSH, and NaSH

molecule	transition[a]	wavelength/nm	oscillator strength
Ag_2S	$a_1 \leftarrow a_1$	390	0.26
	$b_1 \leftarrow a_1$	354	0.62
	$a_1 \leftarrow b_1$	325	0.73
	$b_1 \leftarrow b_1$	300	0.30
AgSH	LUMO ← HOMO-1	276	0.88
NaSH	LUMO+1 ← HOMO	248	0.26

[a] See Figure 10 for the MO diagram of Ag_2S in the HOMO−LUMO region.

consider the electronic transitions of monomers of Ag_2S, AgSH, and NaSH in the UV−vis region. Table 2 lists the optimized geometries used for calculation. There are to our knowledge no experimental results on the structural and electronic properties of these species. Calculations on monomers of Ag_2S in the local density functional approximation yielded smaller bond angles and slightly shorter Ag-S bond lengths than our method (78°/2.33 Å[42] and 86°/2.40 Å[15]). Note that the calculated S−H distances in AgSH and NaSH (see Table 2) correspond well to the experimentally determined value in H_2S (1.3356 Å).[43]

The calculated electronic absorption spectrum of the Ag_2S monomer is essentially composed of 4 transitions between 300 and 400 nm, while the spectrum of AgSH features a single prominent transition at 276 nm. The NaSH monomer is found to absorb at even shorter wavelengths (see Table 3). This is in agreement with the assignment of the experimentally observed bands in the diffuse reflectance spectra of H_2S-loaded NaA and the Ag_2S−NaA samples (see Figures 2 and 1, respectively). Note that we have considered isolated molecules in the calculations. Electronic transitions with participation of the zeolite oxygen lone pairs might become important at higher energies.[10] The occurrence of such transitions strongly depends on the specific coordination of the molecules inside the cavities, which is at present not known. The results of the calculations represent a general trend concerning the energies and intensities of the investigated electronic transitions.

The HOMO of the Ag_2S, AgSH, and NaSH monomers is essentially a 3p(S) orbital. The electronic transition from this

SCHEME 1: Ag_2S−Ag_2S Interaction Geometry

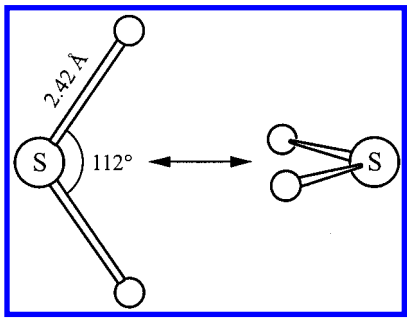

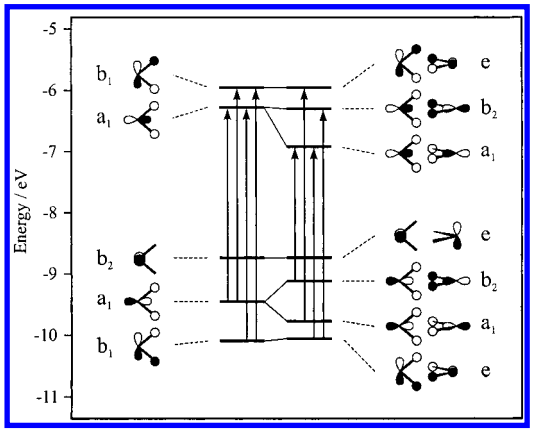

Figure 10. Frontier orbital correlation diagram of Ag_2S (left) and Ag_4S_2 (right). The contribution of the d orbitals to the molecular orbitals is marginal and therefore not shown. Electronic transitions with an oscillator strength larger than 0.01 are indicated by arrows. The HOMO of Ag_2S and also of Ag_4S_2 is located at −8.7 eV.

orbital to the corresponding LUMO generally features oscillator strengths smaller than 0.01. We expect that those transitions are difficult to observe in our diffuse reflectance spectra, but they are essential for the luminescence behavior of the composites. In the case of the Ag_2S monomer the calculated HOMO−LUMO transition is found at 505 nm. This corresponds well to the blue-green emission observed in Ag_2S−NaA and Ag_2S−CaA samples of low silver sulfide content. The nature of the HOMO−LUMO transition is most likely maintained in larger silver sulfide clusters. This explains the significant Stokes shifts which can be observed in the excitation and emission spectra (see Figures 4 and 5) and the comparatively long luminescence lifetimes.

How does the electronic absorption spectrum of a Ag_2S monomer change upon interaction with another Ag_2S monomer, thus forming a Ag_4S_2 cluster? To answer this question, we first have to address the characteristics of this interaction. The appropriate interaction geometry for the two monomers is not immediately evident, mainly because of the yet unknown structure of Ag_4S_2. Starting from the structures proposed by Bagatur'yants et al.,[41] we selected the geometry possessing the highest symmetry, namely, D_{2d} (see Scheme 1). Interaction was studied by reducing the distance between the two Ag_2S monomers. Figure 10 shows the corresponding correlation diagram. While the b_1 and b_2 levels of the monomers are little affected upon interaction, splitting of the two a_1 levels (LUMO and HOMO-1) into levels of b_2 and a_1 symmetry is observed. The thus formed a_1 orbitals are stabilized with respect to the corresponding orbitals in the isolated monomers, while the b_2 orbital that is generated from the HOMO-1 is destabilized. The energy of the b_2 orbital, which is formed upon splitting of the LUMO, is only slightly affected by an alteration of the Ag_2S−Ag_2S distance. The increasingly antibonding s−s and p−p

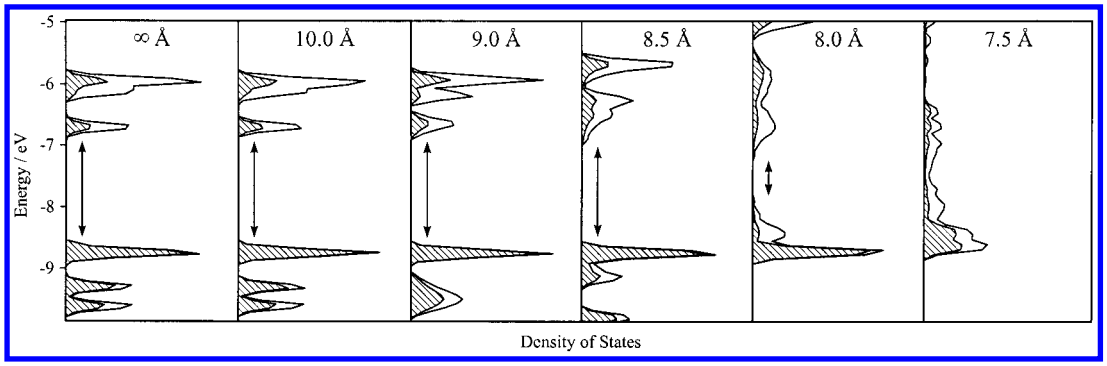

Figure 11. Density of states (DOS) of Ag_4S_2 clusters in a cubic lattice with different lattice constants. The separated system is shown on the left. The band gap of each cluster array is marked by an arrow. The hatched region indicates the contribution of sulfur states.

interaction is in this case compensated by an increasingly bonding s−p interaction. The splitting of the a_1 levels upon interaction leads to a red-shift of the electronic absorption and luminescence bands (note the reduction of the HOMO−LUMO gap). Such a red-shift was also observed in the other geometries leading to the structures described in ref 41.

When dealing with three-dimensional cluster arrays such as the Ag_2S−NaA and Ag_2S−CaA composites the question arises whether the properties of these materials are due to crystal effects originating from interacting clusters. We evaluated the relevance of such effects by calculating the density of states (DOS) of Ag_4S_2 clusters, which are arranged in a cubic lattice. The MO diagram of the Ag_4S_2 cluster used for this purpose is depicted in Figure 10 (right side) with the structure shown in Scheme 1. A S−S distance of 5.6 Å was found to be energetically favorable. The development of the DOS upon variation of the lattice constant is shown in Figure 11. Significant changes can be observed when the lattice constant is smaller than 10 Å. The band gap decreases at values below 9 Å and disappears at 7.5 Å. The distance between the centers of two α-cages in zeolite A is 12.3 Å.[44] The model therefore predicts that there is no through space interaction between the clusters over the whole zeolite crystal up to a loading level of 4 Ag^+ per α-cage. The properties of Ag_2S−NaA-*x* and Ag_2S−CaA-*x* ($x \leq 4$) are therefore mainly determined by the presence of isolated clusters and by short-range interactions between those clusters. Such local interactions are likely to be caused by two clusters located close to a window connecting adjacent α-cages.

Conclusions

The reaction of activated Ag^+-loaded zeolite A with H_2S leads to the formation of silver sulfide clusters in the zeolite cavities. The size of the clusters can thereby be controlled by adjusting the initial Ag^+-loading. Rehydration of the reaction products contributes to the cluster growth by enhancing the mobility of small silver sulfide and silver hydrosulfide species. The thus promoted reaction between AgSH molecules, which are formed at low Ag^+-loading levels, produces Ag_2S and H_2S. The formation of Ag_2S monomers and also of larger silver sulfide clusters is discernible by a band above 300 nm in the diffuse reflectance spectra of the composites. Considering the dimensions of an α-cage of zeolite A, the largest silver sulfide cluster that can be synthesized in such a cavity would have a stoichiometry of approximately Ag_8S_4. Monomers of Ag_2S have to be considered as the smallest clusters. These species are most probably responsible for the blue-green luminescence exhibited by samples of low silver sulfide content. At higher silver sulfide content a luminescence band around 600 nm is observed. The red-shift of this band with increasing silver sulfide loading can be attributed to a quantum size effect.

SCHEME 2: State Diagram for Small Luminescent Silver Sulfide Clusters

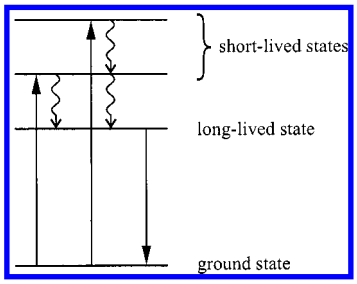

The comparatively long average luminescence lifetimes observed for the orange-red emission in Ag_2S−CaA (e.g., 81 μs for Ag_2S−CaA-2 at −160 °C) and the large Stokes-shifts are in agreement with the results of the MO calculations, which yield small oscillator strengths for the HOMO−LUMO transitions, but very large oscillator strengths for transitions of higher energy. According to these results, a qualitative state diagram can be constructed (see Scheme 2). Because of the inversely proportional relation between the oscillator strength of an electronic transition and the corresponding intrinsic emissive lifetime, the intense absorption transitions give rise to short-lived excited states. Nonradiative relaxation into the lowest excited state is followed by the observed long-lived luminescence.

The properties of the composites are to a certain extent influenced by the co-cations of the zeolite. It is reasonable to assume that the different site occupation patterns of Na^+ and Ca^{2+} in zeolite A play an important role in this context, as they do for the optical properties of Ag^+-loaded zeolite A.[26] The specific mechanism that causes the enhanced luminescence of Ag_2S−CaA (compared to Ag_2S−NaA) is not yet understood. It will for this purpose be necessary to investigate a larger number of different cation-exchanged Ag_2S−zeolite systems.

The Ag_2S−NaA and Ag_2S−CaA host−guest systems constitute three-dimensional quantum dot arrays or quantum lattices. In the case of Ag_4S_2 clusters, coupling over the whole lattice is expected to occur at an average intercluster distance below 10 Å (center to center). We expect that silver sulfide cluster arrays with different structures can be produced by applying the method described in this paper to a variety of zeolites. Comparison of different Ag_2S−zeolite composites would yield further insight into the specific interactions which govern the properties of these host−guest systems. The use of zeolite as host material thereby opens possibilities regarding the assembly of highly organized macroscopic structures. Well-defined close-packed monolayers of high mechanical stability can be prepared on various substrates by using size-selected zeolite A crystals.[23] Furthermore, covalent linkage of zeolite crystals to glass supports allows

the assembly of oriented monolayers[45] and micropatterned structures.[46] Such assemblies are of special interest for the exploitation of the unique optical properties of the Ag_2S−zeolite composites.

Acknowledgment. This work was supported by the Swiss National Science Foundation, project 20-61259.00 and by the Stiftung der Portland Cementfabrik Laufen, Baselland, Switzerland. We thank René Bühler for helpful support in the production of Figure 3.

References and Notes

(1) Nanoscale Materials Special Issue. *Acc. Chem. Res.* **1999**, *32*, 387.
(2) Vossmeyer, T.; Katsikas, L.; Giersig, M.; Popovic, I. G.; Diesner, K.; Chemseddine, A.; Eychmüller, A.; Weller, H. *J. Phys. Chem.* **1994**, *98*, 7665.
(3) Murray, C. B.; Norris, D. J.; Bawendi, M. G. *J. Am. Chem. Soc.* **1993**, *115*, 8706.
(4) van Dijken, A.; Meulenkamp, E. A.; Vanmaekelbergh, D.; Meijerink, A. *J. Lumin.* **2000**, *90*, 123.
(5) Nanda, J.; Sapra, S.; Sarma, D. D.; Chandrasekharan, N.; Hodes, G. *Chem. Mater.* **2000**, *12*, 1018.
(6) Wise, F. W. *Acc. Chem. Res.* **2000**, *33*, 773.
(7) Faraday, M. *Philosoph. Trans.* **1833**, 507.
(8) Sadanaga, R.; Sueno, S. *Mineral. J.* **1967**, *5*, 124.
(9) Junod, P.; Hediger, H.; Kilchör, B.; Wullschleger, J. *Philos. Mag.* **1977**, *36*, 941.
(10) Brühwiler, D.; Seifert, R.; Calzaferri, G. *J. Phys. Chem. B* **1999**, *103*, 6397.
(11) Kitova, S.; Eneva, J.; Panov, A.; Haefke, H. *J. Imaging Sci. Technol.* **1994**, *38*, 484.
(12) Tani, T. *J. Imaging Sci. Technol.* **1995**, *39*, 386.
(13) Mitchell, J. W. *J. Imaging Sci. Technol.* **1998**, *42*, 215.
(14) Charlier, E.; Van Doorselaer, M.; Gijbels, R.; De Keyzer, R.; Geuens, I. *J. Imaging Sci. Technol.* **2000**, *44*, 235.
(15) Baetzold, R. C. *J. Imaging Sci. Technol.* **1999**, *43*, 375.
(16) Motte, L.; Pileni, M. P. *J. Phys. Chem. B* **1998**, *102*, 4104.
(17) Sun, Y.-P.; Riggs, J. E.; Rollins, H. W.; Guduru, R. *J. Phys. Chem. B* **1999**, *103*, 77.
(18) Belous, V. M.; Tolstobrov, V. I.; Sviridova, O. I.; Chibisov, K. V. *Dokl. Phys. Chem. (Engl. Transl.)* **1982**, *262*, 75.
(19) Akamatsu, K.; Takei, S.; Mizuhata, M.; Kajinami, A.; Deki, S.; Takeoka, S.; Fujii, M.; Hayashi, S.; Yamamoto, K. *Thin Solid Films* **2000**, *359*, 55.
(20) Rollins, H. W.; Lin, F.; Johnson, J.; Ma, J.-J.; Liu, J.-T.; Tu, M.-H.; DesMarteau, D. D.; Sun, Y.-P. *Langmuir* **2000**, *16*, 8031.
(21) Brelle, M. C.; Zhang, J. Z.; Nguyen, L.; Mehra, R. K. *J. Phys. Chem. A* **1999**, *103*, 10194.
(22) Henglein, A.; Gutiérrez, M.; Weller, H.; Fojtik, A.; Jirkovský, J. *Ber. Bunsen-Ges. Phys. Chem.* **1989**, *93*, 593.
(23) Lainé, P.; Seifert, R.; Giovanoli, R.; Calzaferri, G. *New J. Chem.* **1997**, *21*, 453.
(24) Li, J. W.; Pfanner, K.; Calzaferri, G. *J. Phys. Chem.* **1995**, *99*, 2119.
(25) Sherry, H. S.; Walton, H. F. *J. Phys. Chem.* **1967**, *71*, 1457.
(26) Seifert, R.; Rytz, R.; Calzaferri, G. *J. Phys. Chem. A* **2000**, *104*, 7473.
(27) Seifert, R.; Kunzmann, A.; Calzaferri, G. *Angew. Chem. Int. Ed.* **1998**, *37*, 1522.
(28) Calzaferri, G.; Giovanoli, R.; Kamber, I.; Shklover, V.; Nesper, R. *Res. Chem. Intermed.* **1993**, *19*, 31.
(29) Hoffmann, R. *J. Chem. Phys.* **1963**, *39*, 1397.
(30) Calzaferri, G.; Forss, L.; Kamber, I. *J. Phys. Chem.* **1989**, *93*, 5366.
(31) Rytz, R.; Glaus, S.; Brändle, M.; Brühwiler, D.; Calzaferri, G. *ICON-EDiT, Extended Hückel Molecular Orbital and Transition Dipole Moment Calculations*; available at http://iacrs1.unibe.ch; Department of Chemistry and Biochemistry, University of Bern: Freiestrasse 3, 3012 Bern, Switzerland, 1997 (update 2000).
(32) Ammeter, J. H.; Bürgi, H.-B.; Thibeault, J. C.; Hoffmann R. *J. Am. Chem. Soc.* **1978**, *100*, 3686.
(33) Brühwiler, D.; Gfeller, N.; Calzaferri, G. *J. Phys. Chem. B* **1998**, *102*, 2923.
(34) Glaus, S.; Calzaferri, G. *J. Phys. Chem. B* **1999**, *103*, 5622.
(35) Basch, H.; Viste, A.; Gray, H. B. *Theor. Chim. Acta* **1965**, *3*, 458.
(36) Calzaferri, G.; Rytz, R. *J. Phys. Chem.* **1995**, *99*, 12141.
(37) Hoffmann, R. *Solids and Surfaces: A Chemist's View of Bonding in eXtended Structures*; VCH: New York, 1988.
(38) Brändle, M.; Rytz, R.; Calzaferri, G. *BICON−CEDiT, Extended Hückel Tight-Binding and Crystal Transition Dipole Moment Calculations;* available at http://iacrs1.unibe.ch; Department of Chemistry and Biochemistry, University of Bern: Freiestrasse 3, 3012 Bern, Switzerland, 1997, update 2000.
(39) Karge, H. G.; Ziólek, M.; Laniecki, M. *Zeolites* **1987**, *7*, 197.
(40) Giggenbach, W. *Inorg. Chem.* **1971**, *10*, 1333.
(41) Bagatur'yants, A. A.; Safonov, A. A.; Stoll, H.; Werner, H.-J. *J. Chem. Phys.* **1998**, *109*, 3096.
(42) Dixon, D. A.; Gole, J. L. *Chem. Phys. Lett.* **1992**, *189*, 390.
(43) Lide, D. R. Ed. *CRC Handbook of Chemistry and Physics*, 77th ed.; CRC Press: Boca Raton, 1996; pp 9-19.
(44) Breck, D. W. *Zeolite Molecular Sieves*; John Wiley: New York, 1974.
(45) Kulak, A.; Lee, Y.-J.; Park, Y. S.; Yoon, K. B. *Angew. Chem. Int. Ed.* **2000**, *39*, 950.
(46) Ha, K.; Lee, Y.-J.; Jung, D.-Y.; Lee, J. H.; Yoon, K. B. *Adv. Mater.* **2000**, *12*, 1614.